Bespoke Biomolecular Wires for Transmembrane Electron Transfer: Spontaneous Assembly of a Functionalized Multiheme Electron Conduit.

Samuel E. H. Piper[1], Marcus J. Edwards[1a], Jessica H van Wonderen[1], Carla Casadevall[2], Anne Martel[3], Lars J. C. Jeuken[4], Erwin Reisner[2], Thomas A. Clarke[1]* and Julea N. Butt[1]*

[1] School of Chemistry and School of Biological Sciences, University of East Anglia, Norwich Research Park, Norwich, NR4 7TJ, UK.

[2] Yusuf Hamied Department of Chemistry, University of Cambridge, Lensfield Road, Cambridge CB2 1EW, UK

[3] Institut Laue-Langevin, 38042 Grenoble, France.

[4] School of Biomedical Sciences, University of Leeds, Leeds, LS2 9JT, UK.

[a] present address: School of Life Sciences, University of Essex, Colchester, CO4 3SQ, UK.

*** Correspondence:**
Julea Butt
j.butt@uea.ac.uk

Thomas Clarke
tom.clarke@uea.ac.uk

Keywords: cytochrome, electron transfer, microbial fuel cell, microbial electrosynthesis, photosensitizer, biomolecular wire, SANS, *Shewanella*.

Abstract

Shewanella oneidensis exchanges electrons between cellular metabolism and external redox partners in a process that attracts much attention for production of green electricity (microbial fuel cells) and chemicals (microbial electrosynthesis). A critical component of this pathway is the outer membrane spanning MTR complex; a biomolecular wire formed of the MtrA, MtrB and MtrC proteins. MtrA and MtrC are decaheme cytochromes that form a chain of close-packed hemes to define an electron transfer pathway of 185 Å. MtrA is wrapped inside MtrB for solubility across the outer membrane lipid bilayer; MtrC sits outside the cell for electron exchange with external redox partners. Here we demonstrate tight and spontaneous *in vitro* association of MtrAB with separately purified MtrC. The resulting complex is comparable to the MTR complex naturally assembled by *Shewanella* in terms of both its structure and rates of electron transfer across the lipid bilayer. Our findings reveal the potential for building bespoke electron conduits where MtrAB combines with chemically modified MtrC, in this case labeled with a Ru-dye that enables light-trigged electron injection into the MtrC heme chain.

1 Introduction

Dissimilatory metal-reducing bacteria (DMRB) are able to gain energy for growth by coupling the oxidation of organic compounds to the reduction of iron and manganese containing minerals. These terminal respiratory electron acceptors are insoluble. They cannot enter the bacterial cell and DMRB have evolved mechanisms to transport electrons out of the cell across otherwise electrically insulating lipid membranes[1-2]. The same mechanisms allow respiration on numerous extracellular electron acceptors including suitably poised electrodes. Thus, DMRB attract much attention for their abilities to deliver clean energy and chemicals [2-5] in addition to their fascinating microbiology.

Shewanella oneidensis MR-1 is a model organism for fundamental and applied studies of DMRB[6-9]. The primary mechanism of electron release from *S. oneidensis* MR-1 is relatively simple, Fig. 1A, and at the molecular level is arguably the best understood of the DMRB. Electrons from the oxidation of organic compounds are transferred via menaquinol to the inner membrane quinol dehydrogenase CymA[10]. Periplasmic cytochromes STC and FccA then transfer electrons from CymA to the outer membrane associated MTR complex[11]. At the cell surface, electrons are transferred from the MTR complex to terminal respiratory acceptors either directly or via flavin mediators[12-13]. Alongside transmembrane electron transfer, the MTR complex is proposed to transport protons across outer membranes as the rate-limiting event[14] during electron transfer from biofilms of *S. oneidensis* to electrodes.

The MTR complex[15] is comprised of three proteins, Fig. 1B. Two of these proteins form an outer membrane spanning complex, MtrAB, which assembles as a naturally insulated biomolecular wire with both a structure and function that are analogous to those of an electrical cable. MtrA binds an approximately linear chain of 10 *c*-type hemes which spans the lipid bilayer. Those hemes are insulated from the membrane by embedding within a 26 strand beta-barrel formed by MtrB. Electrons enter MtrAB at Heme A1 in the periplasm. At the external face of MtrAB, Heme A10 is positioned close to Heme C5 in the decaheme cytochrome MtrC (heme edge-to-heme edge distance of 8 Å)[15]. By this means, electrons can transfer from MtrA to MtrC for distribution across ten hemes and a large surface area of MtrC that can be accessed by extracellular electron acceptors. MtrC may also pass electrons to a homologous extracellular decaheme cytochrome OmcA[16].

Previously we reported[17] that *in vitro* mixing of purified MtrAB and soluble forms of MtrC results in the spontaneous formation of a stable high-affinity complex. Formation of the complex was evidenced by native PAGE and analytical ultracentrifugation with both techniques describing a complex of approximately 210 kDa that is indicative of a 1:1 association of soluble MtrC (approx. 80 kDa) and MtrAB (approx. 120 kDa). However, at that time no information was available on the structure or electron transfer properties of the *in vitro* assembled complex. We address those gaps in knowledge in this report. Utilizing small-angle neutron scattering (SANS), the complex formed spontaneously *in vitro* is shown to have a similar structure to the MTR complex purified directly from *S. oneidensis*, and revealed to be equally effective in the transfer of electrons across lipid bilayers. Our results pave the way for novel synthetic biology approaches to assemble functional MtrC:MtrAB complexes in homologous and heterologous hosts, with the potential to utilize chemically modified MtrC subunits to impart non-native functionality.

2 Materials and Methods

2.1 Protein Purification and Biochemical Analyses

Y657C MtrC, lacking the lipid attachment site of wild-type MtrC and carrying a C-terminal Strep II affinity tag, and MtrAB were purified as previously described[17-19] after overexpression from pBAD2020/TOPO vectors carried by a strain of *Shewanella oneidensis* MR-1 lacking the *mtr* operon. Cys-directed labeling of Y657C MtrC with [Ru(4-bromomethyl-4'-methylbipyridine)(2,2'-bipyridine)$_2$](PF_6)$_2$ (HetCat, Switzerland) was performed as described previously[19-20]. The labeling efficiency was close to 100% as judged by LC-MS and UV-visible absorbance spectroscopy. The Ru-dye labeled protein is termed Ru-MtrC, Fig. S2. For LC-MS, performed as described in Ref.[20], protein (typically >2 mg mL^{-1}) was diluted with formic acid (0.1% v/v) and acetonitrile (2% v/v) prior to analysis.

Protein concentrations were quantified by absorbance spectroscopy of the fully oxidized, air equilibrated proteins with all hemes in the Fe(III) state; for MtrAB using ε_{408nm} = 1 238 000 M^{-1} cm^{-1} and for Ru-MtrC[19] using ε_{408nm} = 1 389 000 M^{-1} cm^{-1}. Extinction coefficients were experimentally determined by the pyridine hemochromagen method[21]. Photoluminescence was measured for anaerobic protein solutions with 50 mM sodium phosphate, 50 mM NaCl, 5 mM lauryldimethylamine oxide (LDAO) (Sigma-Aldrich), pH 7.5 in sealed 1 mL quartz fluorescence cuvettes. Emission spectra were recorded using an excitation wavelength of 460 nm. Measurements were made with a Cary Eclipse Fluorescence Spectrophotometer: excitation slit width, 20 nm; emission slit width, 10 nm; PMT detector voltage, medium.

Gel filtration chromatography was carried out at 4 °C using a Superose 6 Increase 10/300 column (Cytiva) operated by an Äkta Pure chromatography system. The column was equilibrated with 50 mM sodium phosphate, 50 mM NaCl, 5 mM LDAO, pH 7.5 before loading 0.5 mL of protein sample in the same buffer. The sample was eluted at a flow rate of 0.25 mL min^{-1}, eluent was monitored by optical spectroscopy at 410 nm to detect the presence of heme.

2.2 Analytical Ultracentrifugation

Sedimentation equilibrium analytical ultracentrifugation (SE-AUC) experiments were performed using a Beckman Optima XLA-I analytical ultracentrifuge equipped with scanning absorbance optics. Measurements were performed in 50 mM sodium phosphate, 50 mM NaCl, 0.1% (v/v) Triton X-100 (Acros Organics), pH 7.5 for which the density (ρ) was calculated as 1.007 g mL^{-1} using utility software in Ultrascan II[22]. Ultrascan II was also used to calculate the partial specific volume ($\bar{v}$) of each protein: 0.721 for Ru-MtrC, 0.716 for MtrAB, and 0.718 for the Ru-MtrC:MtrAB complex. SE-AUC was performed at 20 °C using speeds of 8k, 10k, and 12k rpm with absorbance profiles recorded at 410 nm. The programme Ultrascan II was used to analyze the sedimentation equilibrium profiles and to fit the data to those predicted for single non-interacting species. Data are presented as R^2- R_{ref}^2 against Ln($A_{410\,nm}$); the gradient of this plot can be used to determine the molecular weight (M_W) of the species by the equation:

$$M_W = \frac{2\boldsymbol{RT}}{(1-\bar{v}\rho)\omega^2} \times \frac{dln(C_r)}{d(R^2 - R_{ref}^2)}$$

where $\boldsymbol{R}$ is the gas constant, T is the temperature, C_r is the sample concentration at radial distance R, R_{ref} is the radial distance of the sample meniscus, and ω is the angular velocity. Radial distance is measured from the axis of rotation.

2.3 SANS Data Collection and Analysis

Ru-MtrC:MtrAB was prepared by combining Ru-MtrC with a slight excess of MtrAB and performing gel filtration chromatography as described above. Ru-MtrC:MtrAB eluting from the Superose 6 Increase 10/300 column with V_e < 16.5 mL, i.e. separated from free MtrAB, was pooled and loaded onto a 5 mL HiTrap Q FF column (Cytiva) equilibrated with 50 mM sodium phosphate, 50 mM NaCl, 5 mM LDAO, pH 7.5. Bound protein was washed with 50 mL of 20 mM HEPES, 100 mM NaCl, 2.8 mM Fos-choline 12 (Anatrace), pH 7.8 at 1 mL min^{-1} to exchange the detergent before elution with 20 mM HEPES, 0.5 M NaCl, 2.8 mM Fos-choline 12, pH 7.8. A 100 kDa molecular weight cut-off spin concentrator (Millipore) was then used to lower the NaCl concentration to 100 mM and concentrate the protein to 10 mg mL^{-1}. Immediately prior to SANS data collection the protein sample was dialyzed overnight in a sealed DURAN bottle containing 20 mM HEPES, 100 mM NaCl, 2.8 mM Fos-choline 12, 13% D_2O, pH 7.8 using a 50 kDa molecular weight cut-off Dispo-Biodialyzer (Merck). By including 13% D_2O, this ensured that the neutron scattering length density of the buffer matches that of Fos-choline 12. This match point was previously determined by a SANS study of MtrAB and the Mtr complex [18]. Protein samples at concentrations of 6.3 and 3.1 mg mL^{-1} were prepared by appropriate dilution using dialysis buffer to ensure precise buffer matching. 200 µL samples were centrifuged at 13 000 ×*g* for 10 min at 4 °C to remove any potentially aggregated material, although no visible pellet was observed, before being sealed in 0.1 cm path-length suprasil quartz cuvettes (Hellma). An aliquot of dialysis buffer was also prepared in the same manner and was measured alongside the protein sample for downstream buffer subtraction.

SANS data were collected on the D22 diffractometer (Institut Laue-Langevin, France) using a neutron beam (λ = 6 Å ± 10%) at three configurations of collimation, 17.6, 8.0 and 2.8 m, and respective detector distances of 17.6, 8.0 and 1.4 m covering Q ranging from 0.003 to 0.6 $Å^{-1}$. The collimation cross-section was 40 mm × 55 mm and the sample aperture was 7 mm × 10 mm. Exposure times ranged from 60 s to 2 h depending on sample concentration, contrast, and instrument configuration. Data reduction was performed using GRASP including blocked beam and empty cell background subtraction, sample thickness and transmission scaling, and calibration to absolute intensity using incident neutron flux at sample position. As the final step azimuthal averaging was performed to output the scattering intensity I(Q).

Data were processed as previously described[18] for the MTR complex. Briefly, curves were merged and buffer subtraction was carried out utilizing IGOR Pro (Wavemetrics) with the NCNR macros installed[23]. The ATSAS software suite[24] was used to analyse the I(Q) curves in order to perform a Guinier analysis to estimate the radius of gyration (R_g) at low Q ($Q_{max} \times R_g < 1.3$), and to produce Kratky plots to evaluate the overall compactness of the protein complexes. GNOM[25] was used to calculate the pair distance distribution function (P(r)) i.e. the Fourier inversion of the scattering intensity, I(Q),which provides an independent estimation of R_g as well as the maximum dimension of the scattering particle $D_{max.}$ Using DAMMIF[26], 20 bead models of the molecule were refined to fit the experimental P(r). The DAMAVER suite of software[27] was then used to create pairwise alignments of all 20 models, identify and remove outliers amongst the models, 2 of the 20 models in this case, and create an average from the remaining 18 models. Reported molecular envelopes were produced by refinement of the averaged model using DAMMIN[28]. A homology model for the MTR complex of *S. oneidensis*, Fig. 1B, was prepared by using Phyre2 to generate a model for MtrAB and combining

that with the crystal structure of *S. oneidensis* MtrC (PDB ID: 4LM8) docked in the same position as MtrC of the *S. baltica* MTR complex (PDB ID: 6R2Q). This homology model was aligned to the SANS molecular envelopes using SUPCOMB[29]. SANS data collection and processing statistics are reported in Table S3.

2.4 Photoreduction of Ru-MtrC and Ru-MtrC:MtrAB Suspensions.

Experiments were performed in anaerobic 50 mM Tris:HCl, 10 mM KCl, 100 mM EDTA, 0.2% (v/v) Triton X-100, pH 8.5. Spectra were recorded in 1 mL SOG cuvettes (Hellma) in a Biochrom WPA Biowave II Diode-array spectrophotometer placed in a N_2-filled chamber (Belle Technology, atmospheric O_2 < 5 ppm). An Omega Optical 475RB Notch filter was used to prevent photoexcitation by the spectrophotometer. The light source for photoreduction was a Thorlabs mounted LED (λ_{max} = 455 nm) (Fig. S1) equipped with a collimator adapter. The excitation intensity at the sample was 110 W m^{-2} (0.42 mE m^{-2} s^{-1}) as determined by potassium ferrioxalate actinometry[30-31]. Samples were irradiated continuously from above and spectra taken at the desired time intervals. The percentage of reduced hemes was quantified using the baseline-corrected absorbance of the heme Soret band at 420 nm. The absorbance prior to irradiation was taken to be of the fully oxidized protein (0% reduced heme). The absorbance of fully reduced protein (100% reduced heme) was obtained at the end of the experiment by addition of an excess of the chemical reductant sodium dithionite.

2.5 Preparation of Liposomes and Proteoliposomes

Liposomes were prepared following an adaptation of the method reported by Stikane et al[32]. 20 mg of Polar lipid extract (Avanti Polar Lipids) was suspended in 750 µL of 50 mM Tris:HCl, 10 mM KCl, 10 mM reactive red 120 (RR120, Sigma-Aldrich), pH 8.5 by vigorous vortexing for 20 min. The suspended lipid was then solubilized by addition of 500 µL of 250 mM octyl glucoside (Anatrace). Proteins were then incorporated by addition of 100 µL of 25 µM protein complex in 50 mM sodium phosphate, 50 mM NaCl, 5 mM LDAO, pH 7.5. Ru-MtrC and MtrAB were mixed to form the Ru-MtrC:MtrAB complex prior to incorporation of this complex into proteoliposomes. For control experiments without proteins, liposomes were prepared by addition (100 µL) of 50 mM sodium phosphate, 50 mM NaCl, 5 mM LDAO, pH 7.5. The resulting mixture was incubated on ice for 20 min before gradual addition, over 2 min, to ice cold 50 mM Tris:HCl, 10 mM KCl, 10 mM RR120, pH 8.5 to give a final volume of 50 mL. This dilution lowered the octyl glucoside concentration below its critical micelle concentration resulting in liposome formation with spontaneous protein integration and RR120 encapsulation.

The dilute liposome suspension was subject to ultracentrifugation at 205 000 ×*g* for 1h to pellet the liposomes. After removal of the supernatant, pellets were transferred to a N_2-filled chamber and resuspended in 50 mL of anaerobic 50 mM Tris:HCl, 10 mM KCl, pH 8.5. The liposome pellets recovered after a second ultracentrifugation, as above, were then resuspended to a final volume of 1 mL in anaerobic 50 mM Tris:HCl, 10 mM KCl, pH 8.5 and allowed to equilibrate overnight at room temperature in the anaerobic chamber. The liposome concentration of these samples was approx. 300 nM, estimated on the basis of the liposome dimensions (see below) and lipid composition as described in the SI.

Dynamic light scattering was used to assess the dimensions of the liposomes in samples containing approx. 6 nM liposome in 50 mM Tris:HCl, 10 mM KCl, pH 8.5. Measurements used a Zetasizer Nano with DTS1070 folded capillary cells (Malvern Panalytical) and zeta potentials were measured using the same equipment. Samples were equilibrated at 25 °C for 2 min prior to measurement and

the solvent viscosity was considered to be that of water. The identity of proteins in each of the samples was confirmed using SDS-PAGE with proteins visualized by heme[33] or Coomassie stain.

2.6 Transmembrane Electron Transfer in (Proteo-)Liposomes

Bleaching of encapsulated RR120 was used to monitor transmembrane electron transfer with (proteo-)liposomes as illustrated schematically in Fig. 1C. All experiments were performed inside a N_2-filled chamber (Belle Technology, atmospheric O_2 < 5 ppm). For experiments with sodium dithionite as the electron donor, a stock solution (20 mg mL^{-1}) was prepared by dissolving the required mass in anaerobic 50 mM Tris:HCl, 10 mM KCl, pH 8.5. Then sodium dithionite was added (approx. 0.1 mM final concentration) to anaerobic suspensions of (proteo-)liposomes (approx. 6 nM) containing RR120 in anaerobic 50 mM Tris:HCl, 10 mM KCl, pH 8.5 in 1 mL SOG cuvettes. Absorbance spectra were measured over 5 min. Finally, Triton X-100 was added to 0.2% (v/v) to lyse the liposomes. In all cases this final step led to rapid bleaching of all RR120 present and demonstrated the presence of excess reductant.

Photochemically driven transmembrane electron transfer was monitored by a similar method using graphitic N-doped Carbon Dots as described in Ref [34] and Fig. S3. Prior to use the graphitic N-doped Carbon Dots were suspended to 1 mg mL^{-1} in anaerobic 50 mM Tris:HCl, 10 mM KCl, pH 8.5. For photo-reduction, anaerobic samples in 1 mL SOG cuvettes contained approx. 6 nM (proteo-)liposomes with encapsulated RR120, 10 μg mL^{-1} of graphitic N-doped Carbon Dots and 25 mM EDTA in 50 mM Tris:HCl, 10 mM KCl, pH 8.5. Samples were irradiated by visible-light ($\lambda > 400$ nm) from the side using a Krüss cold light source (Fig. S1) with a fiber optic light pipe as described in Ref [35]. Light intensity was measured at 2.5 kW m^{-2} using an Amprobe Solar-100 solar power meter.

Absorbance spectra were measured at desired times with a Biochrom WPA Biowave II diode array spectrophotometer. Raleigh scattering due to the liposomes was calculated using the equation:

$$Scattering\ intensity = A + {}^{B}/_{\lambda^4}$$

and subtracted from the measured data. For each series of experiments the variables A and B were adjusted to give a good fit to the measured data where absorbance from protein and dye were minimal; below 260 nm and above 640 nm (e.g. Fig. S4). Dye absorbance was then quantified at 539 nm, a wavelength which is isosbestic with respect to heme oxidation state[32].

3 Results and Discussion

MtrAB when purified and resuspended in detergent micelles was previously[17] shown to bind to separately purified soluble forms of MtrC but not OmcA, which is an extracellular decaheme cytochrome of *S. oneidensis* homologous to MtrC. This selective binding led us to anticipate that the MtrC:MtrAB complex would have a structure similar to that of the MTR complex. MtrC Heme C5 would be positioned close to MtrAB Heme A10, Fig. 1B, and the environment of MtrC Heme C10 would be the same in purified MtrC as in the MTR complex. Labeling the surface of MtrC near Heme C10 with a luminescent dye would provide the opportunity to report on that local environment. If, in addition, that dye could transfer photo-energized electrons to the MtrC hemes there might be opportunities to probe MtrC to MtrAB electron transfer within the MtrC:MtrAB complex following light-triggered electron injection into MtrC Heme C10.

The thiol-reactive dye [Ru(4-bromomethyl-4'-methylbipyridine)(2,2'-bipyridine)$_2$](PF_6)$_2$[36-37] has been successfully attached to cysteine residues on the surfaces of a number of redox proteins. This dye has a well-characterized luminescence that is sensitive to local environment[20]. Furthermore, the photoexcited dye is capable of injecting photoenergized electrons into multiheme cytochromes including *S. oneidensis* STC[20, 38] and of PpcA of *Geobacter sulfurreducens*[39]. Thus, we prepared[19] a soluble MtrC variant with Tyr657 replaced by Cys on the surface of MtrC at a site close to Heme C10, Fig. 1B. Cys657 was then labeled by reaction with [Ru(4-bromomethyl-4'-methylbipyridine)(2,2'-bipyridine)$_2$](PF_6)$_2$ to form a protein, here termed Ru-MtrC, that retains the spectral and redox properties of the hemes in the native protein[19].

As described below, Ru-MtrC forms a 1:1 complex when mixed with MtrAB. The structure of the resultant complex, termed Ru-MtrC:MtrAB, was assessed by analytical ultracentrifugation, gel-filtration chromatography, SANS and luminescence spectroscopy. Electron transfer was probed by optical spectroscopy of the complex in detergent micelles and incorporated in lipid bilayers.

3.1 Oligomeric State and Solution Structure of the Ru-MtrC:MtrAB Complex

SE-AUC provides a direct measure of the average mass of proteins in solution[40]. As a consequence their oligomeric state can be readily defined and SE-AUC was the method of choice for initial characterization of samples containing Ru-MtrC, MtrAB and 1:1 mixtures of Ru-MtrC with MtrAB. Data were collected at three rotation speeds for each sample. In each case the absorbance profile indicative of protein concentration across the sample, e.g. Fig. 2A, was well-described by the behavior predicted for a single, non-interacting species. For Ru-MtrC (0.4 μM) the apparent mass was 82 400 Da and for MtrAB (0.4 μM) it was 120 000 Da. These values are in good agreement with those of 76 788 and 114 047 Da calculated for Ru-MtrC and MtrAB, respectively, on the basis of primary sequence, covalent modification by ten *c*-type hemes, and labeling of the former protein with the Ru-dye. It was concluded that Ru-MtrC and MtrAB are monomer and heterodimer, respectively, under the experimental conditions.

Analysis of the absorbance profiles for samples containing MtrAB (0.25 μM) and an equal concentration of Ru-MtrC revealed a single homogeneous species with an apparent molecular mass of approx. 204 000 Da. This mass is comparable to the sum (190 835 Da) of those for Ru-MtrC and MtrAB. Thus, Ru-MtrC combines with MtrAB to form a heterotrimer having a 1:1 ratio of Ru-MtrC and MtrAB. We note that all samples contained 0.1% (v/v) of the detergent Triton X-100, to maintain solubility of the membrane proteins, and that the approximate micellar weight for Triton X-100 is 80 kDa. However, there is negligible micellar contribution to the overall mass for proteins of the size studied here. This is because the partial specific volume of Triton X-100 (0.91 mL g^{-1})[41] is close to that of the buffer-electrolyte (0.99 mL g^{-1}) such that the micelle is only weakly affected by the centrifugal force. The proteins, by comparison, have partial specific volumes of approx. 0.72 mL g^{-1}.

Further evidence for spontaneous formation of a tight, stable complex between Ru-MtrC and MtrAB was provided by analytical gel filtration chromatography, Fig. 2B. Resolution was afforded by a Superose 6 Increase column for samples having a concentration approximately 100× greater than used for SE-AUC analysis. Ru-MtrC eluted as a single peak centered on an elution volume (V_e) of approx. 17.8 mL and samples of the higher mass MtrAB complex eluted as a single peak centered on V_e approx. 17.1 mL. A sample containing Ru-MtrC (32 μM) equilibrated with an excess of MtrAB (48 μM) eluted as two peaks. The smaller peak, centered on V_e approx. 17.1 mL, is assigned to excess MtrAB. The larger peak, centered on V_e approx. 15.9 mL, is assigned to a species of higher molecular mass that we consider to be the Ru-MtrC:MtrAB complex. This interpretation was

supported by SDS-PAGE, Fig. 2C, of material with V_e approx. 15.5 mL where bands with the expected mass of Ru-MtrC, MtrA and MtrB were observed.

Previously[18] we used SANS to resolve the molecular envelopes of MtrAB and the MTR complex purified from *S. oneidensis*. For those experiments, proteins were suspended in a buffer containing Fos-choline 12 detergent and 13% D_2O in order to match the neutron scattering length density of both detergent micelles and bulk buffer solution. Upon buffer subtraction the scattering intensity profile of the detergent micelles is also subtracted revealing the neutron scattering intensity profile from the protein complexes alone. We used the same approach here to resolve the molecular envelope of Ru-MtrC:MtrAB. We note that our ability to prepare Ru-MtrC:MtrAB in Triton X-100 (SE-AUC), LDAO (gel filtration) and Fos-choline 12 (SANS) highlights the stability of the complex in a range of detergents.

Neutron scattering data were collected for Ru-MtrC:MtrAB at concentrations of 6.3 and 3.1 mg mL^{-1}. The scattering intensity profiles scaled linearly with protein concentration indicating an absence of concentration dependent interparticle interactions (Fig. S5). The scattering curves were merged, providing a curve, Fig. 3A, with high reliability and signal-to-noise. Guinier analysis, Fig. 3B, produced a linear plot indicating that the samples of Ru-MtrC:MtrAB were not aggregated and had an approximate radius of gyration (R_g) of 46.9 $\pm$ 0.6 Å. A Kratky plot ($I(Q) \times Q^2$ versus Q, where I(Q) is the intensity at a given scattering distance and Q is momentum transfer), Fig. 3C, indicated Ru-MtrC:MtrAB was globular. P(r) distance distribution curves were generated using the GNOM program based on inverse Fourier transform of the data to a maximum Q value of 0.161 $Å^{-1}$. The scattering intensity decreased significantly beyond this value, so data were truncated before calculation of P(r) distribution curves. The P(r) curve shape, Fig. 3D, was suggestive of a globular protein with a maximum distance in the molecule, D_{max}, of 166 Å and an R_g of 48.2 Å. The latter is in good agreement with the value determined by Guinier analysis (see above). The theoretical scattering produced by this P(r) curve fits well to the experimental scattering data, Fig. 3A, with a χ^2 of 0.764 as determined by GNOM.

The P(r) curve was used to produce *ab initio* structural models for Ru-MtrC:MtrAB using DAMMIF[26]; these were then processed with DAMAVER[27] as previously described[18]. Final refinement using DAMMIN[28] produced a molecular envelope which is shown in Fig. 3E. It has been aligned, using SUPCOMB[29], to the homology model for the *S. oneidensis* MTR complex (Fig. 1B) generated based upon the crystal structure of the MTR complex from *S. baltica* OS185[15] and the structure of MtrC from *S. oneidensis* MR-1[42]. The theoretical scattering profile produced by this molecular envelope had a χ^2 value of 2.748 (determined by DAMMIN) against the original scattering curve (Fig. S6F) indicating a good fit to the data and the alignment had a normalized spatial discrepancy (NSD) of 2.05. The data reveal agreement between the Ru-MtrC:MtrAB molecular envelope from SANS and the homology model for the MTR complex at the level of resolution afforded by SANS.

The scattering data obtained previously[18] for the MTR complex was subject to the same analysis and modeling comparable to that described above for Ru-MtrC:MtrAB (Fig. S6). The final molecular envelope for the MTR complex had a χ^2 value of 1.972 (determined by DAMMIN) against the scattering data (Fig. S6F) and alignment to the homology model for *S. oneidensis* MTR complex gave a NSD of 2.72 (Fig. S6E). The DAMMIN models of the Ru-MtrC:MtrAB and MTR complexes are compared in Fig. 3F and reveal very similar global structures at the resolution provided by SANS. Both models align similarly well with the homology model for the MTR complex generated from the crystal structure[15] of the complex from *S. baltica*. This finding gives confidence in the homology

model generated to describe the structure of the *S. oneidensis* MTR complex. In addition it reveals that the MTR solution structure is not significantly different to that resolved in a crystalline state.

SANS analysis of Ru-MtrC:MtrAB lacks the resolution required to locate the Ru-dye attached to MtrC Cys657. To confirm the dye is positioned away from the interface between MtrC and MtrAB, as expected from the structure of the MTR complex Fig. 1B, the spectral properties of the dye attached to MtrC were investigated in the absence and presence of MtrAB. If MtrC Heme C10 is located near the interface with MtrAB we can expect this to impact the photoluminescence intensity or spectral profile of the Ru-dye. However, there was negligible change to the emission spectrum of 1 μM Ru-MtrC after incubation with 0.5, 1 or 2 μM MtrAB over a 5 h period (Fig. S7). These observations are consistent with a 'correct' relative orientation of Ru-MtrC and MtrAB such that Heme C10 is positioned some distance from MtrAB, Fig. 1B.

3.2 Electron Transfer Through the Ru-MtrC:MtrAB Complex

SANS analysis suggests Ru-MtrC:MtrAB assembles in either the same or a highly similar manner to the wild-type MTR complex assembled in the outer membrane of *Shewanella*. To further investigate the *in vitro* assembled Ru-MtrC:MtrAB complex a series of experiments explored the electron transfer properties. Initial investigations took advantage of the Ru-dye attached to MtrC. The photoexcited triplet state of this dye, generated by absorption of photons at blue wavelengths, is a strong reductant (E_m approx. -830 mV vs SHE) with a lifetime of approx. 600 ns that is capable of transferring its photoenergized electron to a nearby protein cofactor e.g. [19-20, 36-38]. The photoenergized electron becomes trapped in the protein if the oxidized dye is reduced by a sacrificial electron donor, and provided there are no sacrificial acceptors present. For cytochromes with multiple hemes such photoreduction is cumulative[20] and readily quantified by changes in absorbance of the Soret band as illustrated for Ru-MtrC, e.g. Fig. 4A. Initially the protein is fully oxidized with all hemes in the Fe(III) state as indicated by the Soret band with maximum absorbance at 410 nm, Fig.4A thick red line. Upon irradiation (λ = 455 nm) in the presence of EDTA as sacrificial electron donor the Soret band was red-shifted and gained intensity, Fig. 4A thin red lines. These changes revealed the formation of reduced Fe(II)-containing hemes. Fully reduced Ru-MtrC with ten Fe(II) hemes produced on equilibration with an excess of the chemical reductant sodium dithionite has an intense Soret band with maximum absorbance at 420 nm, Fig. 4A black line.

Cumulative photoreduction of Ru-MtrC:MtrAB was observed during equivalent experiments, e.g. Fig. 4B. Of significance was the finding that for this complex approx. 20 min irradiation was sufficient to drive the reduction of >10 hemes per molecule of Ru-dye. It can be concluded that Ru-MtrC transfers electrons to MtrAB. Reduction was not detected in the absence of EDTA, without irradiation, and without the Ru-dye allowing us to propose a likely mechanism for the cumulative photoreduction, Scheme 1. In Scheme 1 the excited state Ru-dye is presented as $^{*}Ru^{2+}$, the box represents MtrC (or MtrC:MtrAB), D is the sacrificial electron donor EDTA and only productive steps for cumulative photoreduction are illustrated.

Scheme 1.

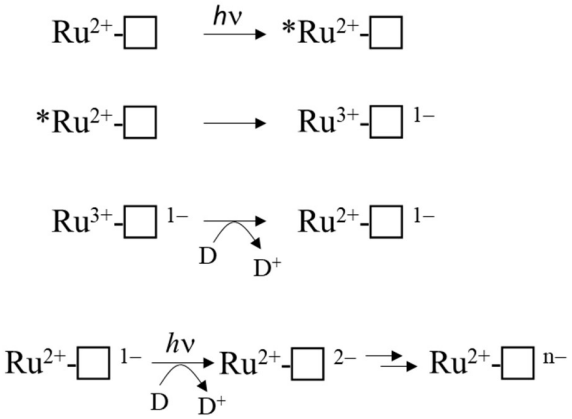

A striking feature of the time courses for photoreduction of MtrC and MtrC:MtrAB is that the maximum (i.e. initial) rates are of the order of 1 heme min^{-1} despite predicted[43-44] and measured[19] heme-to-heme electron transfer rates > μs^{-1}. Similar behavior was described[20, 38] for the tetraheme cytochrome STC of *S. oneidensis* labeled in a manner comparable to that for Ru-MtrC described here. This situation points towards rate-limiting events that involve the Ru-dye, e.g. photoexcitation, EDTA oxidation and/or charge separation (recombination). However, further investigation of these possibilities falls beyond the scope of this present study.

The timescale of cumulative photoreduction reported in this study makes it difficult to confidently distinguish the contribution of electron transfer within Ru-MtrC:MtrAB from that due to electron transfer between such complexes. To overcome this difficulty and provide a description of electron transfer through Ru-MtrC:MtrAB we incorporated the complex into liposome bilayers. The proteoliposomes, illustrated schematically in Fig. 1C, contained RR120 an azo-dye that undergoes reductive bleaching ($E_m \leq$-0.4 V vs SHE) to provide a readily quantified spectroscopic indicator of electron transfer into the proteoliposomes[32].

Proteoliposomes loaded with RR120 were prepared as described in the Methods. SDS-PAGE confirmed that the proteins added during liposome formation were retained in the samples used to study electron transfer, Fig. 5 inset. The presence of encapsulated RR120 was confirmed by a large peak from 460-570 nm in the absorbance spectra, Fig. 6A,B, alongside a smaller Soret peak at 410 nm from Fe(III) heme. Deconvolution of these spectral features allowed the concentrations of dye and Mtr proteins to be calculated (Fig. S4 & Table S2) and demonstrated that the ratio of complex to dye in both types of proteoliposome were similar (approx. 1:270). Dynamic light scattering revealed the size distributions of the proteoliposomes were independent of the incorporated protein, Fig. 5. Zeta potential measurements gave values between -40 and -45 mV with no discernable dependence on the presence, or absence of Mtr proteins. This finding is consistent with our estimate of <5 complexes per liposome, Table S2, with the complex having a footprint of approx. 40 nm^2 in comparison to a proteoliposome surface area of approx. 30 000 nm^2.

The 8 electrons necessary to reduce RR120 and its small extinction coefficient ($\varepsilon_{539\ nm}$ = 32.3 mM^{-1} cm^{-1}) combined with the slow cumulative photoreduction rates for Ru-dye irradiation described above made it necessary for us to use different electron delivery systems with the (proteo-)liposomes. We chose the reductants for their previously described[32] ability to produce rapid (< 10 min) bleaching of internalized RR120 in MTR containing proteoliposomes. Addition of sodium dithionite

to proteoliposomes containing Ru-MtrC:MtrAB or the MTR complex resulted in a rapid bleaching of the internalized RR120, Fig. 6A,B,D. In the absence of Mtr proteins, there was very little bleaching of the dye over the same time period, Fig. 6 C,D. Thus, Ru-MtrC:MtrAB is an effective conduit for electron transfer across the lipid bilayer. Furthermore the rate of electron transfer through Ru-MtrC:MtrAB is comparable to that of the MTR complex, Fig. 6D.

A final series of experiments explored the ability of graphitic N-doped Carbon Dots to support light-driven transmembrane electron transfer. These nanoparticles support rapid photoreduction when irradiated with white light ($\lambda > 400$ nm) in the presence of EDTA as sacrificial electron donor[34]. When our RR120 proteoliposomes containing Ru-MtrC:MtrAB or MTR complex were irradiated in the presence of EDTA the rapid bleaching of RR120 was observed, Fig. 7A,B. The complexes supported comparable rates of bleaching indicative of equivalent rates of electron transfer through Ru-MtrC:MtrAB and the MTR complex. Photoreduction of the Mtr hemes was also apparent through changes in the Soret band, specifically the red shift and increase of intensity. Almost all hemes appeared to be reduced in the first minute, indicating that electron transfer between (Ru-)MtrC and MtrAB is fast compared to the reduction of RR120. In the absence of Mtr proteins, liposomes containing RR120 showed very little evidence for dye bleaching over the same time period, Fig. 7C. Thus, bleaching of the dye is dependent on electron transfer through the Mtr biomolecular wires.

Equivalent experiments performed in the absence of Carbon Dots or EDTA showed negligible reduction of heme and no bleaching of the encapsulated RR120 (Fig. S8). Furthermore, there is no detectable increase in the rate of RR120 bleaching in Ru-MtrC:MtrAB liposomes compared to MTR liposomes, Fig. 7D. We conclude that Ru-MtrC makes very little contribution to photochemical electron production in these experiments and that Carbon Dots are the primary driver of the observed photochemistry.

By two methods of analysis we find that trans-membrane electron transfer by the Ru-MtrC:MtrAB complex is comparable to that by the MTR complex. This supports Ru-MtrC:MtrAB having a structure comparable to that of the MTR complex of *S. baltica*, Fig. 1B, where MtrA Heme A10 and MtrC Heme C5 lie in close proximity to facilitate electron transfer across the interface between the two decaheme cytochromes. We note that the orientation(s) of the complexes in the proteoliposome membranes is not known. However, this is unlikely to affect our conclusions. Given the demonstrated similarity in structure of the MTR complex and Ru-MtrC:MtrAB we expect that the populations of "inside-out" and "right-side-out" complex are similar for each type of proteoliposome. Both orientations are likely to occur as the protein complexes are present during formation of the liposome bilayers.

4 Discussion

An increasing number and diversity of organisms are recognized to naturally transfer electrons between internal enzymes and external redox partners[1, 45]. The electron transfer pathways, evolved to allow survival in the absence of cell permeable electron acceptors, now inspire biotechnology to produce green energy and/or chemicals from material typically considered as waste. Examples include the remediation of water-borne organic 'waste' molecules coupled to electricity production in microbial fuel cells, and the microbial electrosynthesis of valued chemicals from CO_2 and N_2 driven by electricity from renewable sources.[46] These strategies rely on electron exchange between bacteria and electrodes. However, until recently there has been very little molecular understanding of the proteins essential for electron exchange across bacterial outer membranes. It is now apparent that outer membrane-spanning complexes with a *c*-type cytochrome inside a beta-barrel porin protein

play a major role in such electron transfer for numerous and phylogenetically diverse Gram-negative bacteria[1, 15, 47]. Biochemical details are beginning to emerge for the porin-cytochrome fusion exemplified by CYC2 of *Acidithiobacillus ferroxidans*[48-49], the PioAB proteins of *Rhodopseudomonas palustris* TIE-1[50-51], and the PCA complexes of *Geobacter sulfurreducens*[52]. However, it is for *Shewanella* species that trans-outer membrane electron transfer is perhaps best described at the molecular level, e.g. Fig. 1A, B. Notably, the MTR complex provides the primary, and bidirectional, route for electron transfer across the bacterial outer membrane[7, 53].

Recent resolution of the molecular structure of an MTR complex[15] paves the way for its rational engineering to facilitate electrical interfacing of *Shewanella*, or heterologous hosts, with external redox partners. The present study was informed by that structure. We have engineered MtrC for photoreduction by labeling the external surface with a Ru(II)-dye photosensitizer adjacent to the terminal Heme C10. Photoenergized electrons transfer from the dye to MtrC, and subsequently to MtrAB. Furthermore the bespoke biomolecular wire created by mixing water soluble Ru-MtrC with the lipid soluble MtrAB porin:cytochrome complex is indistinguishable from purified MTR in both its structure and ability to transfer electrons across lipid bilayers. Our results can now inform the engineering of bacteria for inclusion in novel biohybrid materials with bespoke transmembrane biomolecular wires. Not only do they provide insight into the cellular pathway for MTR assembly. They suggest bespoke MTR complexes may be assembled in a modular fashion on the surface of live bacteria. We consider both topics below.

Precise details of the cellular MTR assembly pathway are lacking at the present time. In MR-1 the *mtrC*, *mtrB* and *mtrA* genes encoding for the components of the MTR complex are co-transcribed. The translated peptides are transported in an unfolded state, through the Sec pathway, into the periplasm. The *Shewanella* cytochrome *c* maturation pathway folds MtrA and MtrC and attaches ten hemes to each protein[54]. MtrB is then combined with periplasmic MtrA to form the MtrAB complex through a process that may be initiated in the periplasm[55]. By contrast the type II secretion pathway secretes folded MtrC[56] to the external cell surface where it resides as a lipoprotein[57]. The MTR complex forms when the lipoprotein MtrC, anchored to the external cell surface, associates with MtrAB in the outer membrane. By demonstrating that soluble MtrC, lacking the N-terminal lipid attachment site[17], associates with MtrAB to form a complex indistinguishable from MTR, this study reveals that the interfacial contacts between MtrC and MtrAB are sufficient to define and stabilize a functional complex. The lipid anchor carried by genomically encoded MtrC appears to have no structural role. That anchor may ensure that secreted MtrC, synthesized in a process requiring significant investment of cellular resources, diffuses only across the cell surface, essentially in 2D, until it encounters and associates with the MtrAB complex to then perform its role in anaerobic respiration.

With regard to developing novel biotechnology for greener chemical synthesis much inspiration is provided by bacteria, such as *S. oneidensis* MR-1, which naturally couple internal and external redox processes. For example, electrons derived from lactate oxidation by *S. oneidensis* MR-1, Fig. 1A, have been delivered[58] to an exogenous extracellular catalyst for atom-transfer radical polymerization, Fig. 8A. Separately, genetic engineering of *S. oneidensis* introduced new metabolism and demonstrated the production of value-added substances more oxidized than the substrates, Fig. 8B, when glycerol was converted to ethanol[59] and acetoin produced from glucose[8]. Both studies benefited from electrode-assisted fermentation with the liberated electrons passed to anodes. In the future we envisage value-adding half-reactions inside the bacteria will be coupled to value-adding half-

reactions that occur outside the cells such that the concepts above are integrated in a single biotechnology. In such a scenario the performance may be enhanced if MtrC is functionalized with the external electrocatalyst to facilitate electron exchange with the cells. Furthermore, using external photo-electrocatalysts will have the additional advantage of allowing reactions to be driven by the energy of sunlight to achieve semi-artificial photosynthesis in a living organism, Fig. 8C.

While such opportunities are exciting, the direct labelling of bacteria with (photo-)electrocatalysts is likely to provide a challenge, not least the possibility that labelling reactions might compromise cell viability. By demonstrating spontaneous formation of a stable and functional complex able to transfer electrons across a lipid bilayer, this work suggests an alternative route to assembling such biohybrids, Fig. 8C/D. In the first step selective *in vitro* functionalization of purified, soluble MtrC would be carried out under optimal conditions. Then, spontaneous association of functionalized MtrC with cells presenting MtrAB in their outer membrane would afford assembly of the desired biohybrid materials through a strategy that makes a virtue of the intrinsic modularity of the MTR complex. With regards to this strategy, do conditions exist whereby functional MtrC:MtrAB complexes can be assembled by combining soluble, functionalized MtrC with bacteria presenting MtrAB in their outer membranes? Experiments to assess this possibility are ongoing in our laboratories. We also aim to engineer the coupling of MtrC to photosensitizers more sustainable than Ru(II)-dyes, and that support faster light-driven electron accumulation in the protein.

In conclusion we have demonstrated photoreduction of MtrC photosensitized by covalent linkage to an inorganic dye. We have also established that the structure and electron transfer properties of the complex formed when functionalized MtrC associates with MtrAB in vitro are comparable to those of the native MTR complex. Together these observations lay the foundations for rational engineering of the MtrC:MtrAB complex for novel synthetic biology for enhanced biotechnology of *Shewanella* and heterologous hosts such as *E. coli* [60-61].

5 Conflict of Interest

The authors declare that the research was conducted in the absence of any commercial or financial relationships that could be construed as a potential conflict of interest.

6 Author Contributions

J.N.B., T.A.C., S.E.H.P., L.J.C.J and E.R. designed research; S.E.H.P., M.J.E., J.H.W. and A.M. performed research; C.C. provided carbon dots; S.E.H.P., J.H.W., M.J.E., A.M. and T.A.C. analyzed data; J.N.B, S.E.H.P., M.J.E. and T.A.C. wrote the paper. All authors provided critical feedback on the results and manuscript.

7 Funding

Funding was from the UK Biotechnology and Biological Sciences Research Council (BB/S002499/1, BB/S00159X/1, BB/S000704, BB/P01819X/1 and a Doctoral Training Partnership PhD studentship to SEHP) and Engineering and Physical Sciences Research Council (EP/M001989/1). Beamtime 8-03-986 was awarded for work at ILL (Grenoble, France). Access to Transmission Electron

Microscopy was provided through the EPSRC Multi-User Equipment Call (EP/P030467/1). Open access funding was provided by EP/W523288/1.

8 Acknowledgments

We thank Dr Simone Payne for assistance with protein purification and Dr Sam Rowe for spectral characterization of the lights used for irradiation.

9 References

1. White, G.F., Edwards, M.J., Gomez-Perez, L., Richardson, D.J., Butt, J.N. and Clarke, T.A., (2016). Mechanisms of bacterial extracellular electron exchange. Adv. Microb. Physiol. 68, 87-138.

2. Santoro, C., Arbizzani, C., Erable, B. and Ieropoulos, I., (2017). Microbial fuel cells: from fundamentals to applications. A review. J. Power. Sources 356, 225-244.

3. Kato, S., (2015). Biotechnological aspects of microbial extracellular electron transfer. Microbes Environ. 30, 133-139.

4. Nealson, K.H., (2017). Bioelectricity (electromicrobiology) and sustainability. Microb. Biotechnol. 10, 1114-1119.

5. Schroder, U., Harnisch, F. and Angenent, L.T., (2015). Microbial electrochemistry and technology: terminology and classification. Energy Environ. Sci. 8, 513-519.

6. Fredrickson, J.K., Romine, M.F., Beliaev, A.S., Auchtung, J.M., Driscoll, M.E., Gardner, T.S., Nealson, K.H., Osterman, A.L., Pinchuk, G., Reed, J.L., Rodionov, D.A., Rodrigues, J.L.M., Saffarini, D.A., Serres, M.H., Spormann, A.M., Zhulin, I.B. and Tiedje, J.M., (2008). Towards environmental systems biology of *Shewanella*. Nat. Rev. Microbiol. 6, 592-603.

7. Shi, L., Rosso, K.M., Clarke, T.A., Richardson, D.J., Zachara, J.M. and Fredrickson, J.K., (2012). Molecular underpinnings of Fe(III) oxide reduction by *Shewanella oneidensis* MR-1. Front. Microbiol. 3, DOI: 10.3389/fmicb.2012.00050.

8. Bursac, T., Gralnick, J.A. and Gescher, J., (2017). Acetoin production via unbalanced fermentation in *Shewanella oneidensis*. Biotechnol. Bioeng. 114, 1283-1289.

9. Breuer, M., Rosso, K.M., Blumberger, J. and Butt, J.N., (2015). Multi-haem cytochromes in *Shewanella oneidensis* MR-1: structures, functions and opportunities. J. R. Soc. Interface 12, 20141117.

10. McMillan, D.G.G., Marritt, S.J., Butt, J.N. and Jeuken, L.J.C., (2012). Menaquinone-7 is specific cofactor in tetraheme quinol dehydrogenase CymA. J. Biol. Chem. 287, 14215-14225.

11. Sturm, G., Richter, K., Doetsch, A., Heide, H., Louro, R.O. and Gescher, J., (2015). A dynamic periplasmic electron transfer network enables respiratory flexibility beyond a thermodynamic regulatory regime. ISME J. 9, 1802-1811.

12. Marsili, E., Baron, D.B., Shikhare, I.D., Coursolle, D., Gralnick, J.A. and Bond, D.R., (2008). *Shewanella* secretes flavins that mediate extracellular electron transfer. Proc. Natl. Acad. Sci. U.S.A. 105, 3968-3973.

13. von Canstein, H., Ogawa, J., Shimizu, S. and Lloyd, J.R., (2008). Secretion of flavins by *Shewanella* species and their role in extracellular electron transfer. Appl. Environ. Microb. 74, 615-623.

14. Okamoto, A., Tokunou, Y., Kalathil, S. and Hashimoto, K., (2017). Proton transport in the outer-membrane flavocytochrome complex limits the rate of extracellular electron transport. Angew. Chem. 56, 9082-9086.

15. Edwards, M.J., White, G.F., Butt, J.N., Richardson, D.J. and Clarke, T.A., (2020). The crystal structure of a biological insulated transmembrane molecular wire. Cell 181, 665-673.

16. Shi, L., Chen, B.W., Wang, Z.M., Elias, D.A., Mayer, M.U., Gorby, Y.A., Ni, S., Lower, B.H., Kennedy, D.W., Wunschel, D.S., Mottaz, H.M., Marshall, M.J., Hill, E.A., Beliaev, A.S., Zachara, J.M., Fredrickson, J.K. and Squier, T.C., (2006). Isolation of a high-affinity functional protein complex between OmcA and MtrC: Two outer membrane decaheme *c*-type cytochromes of *Shewanella oneidensis* MR-1. J. Bacteriol. 188, 4705-4714.

17. Lockwood, C.W.J., van Wonderen, J.H., Edwards, M.J., Piper, S.E.H., White, G.F., Newton-Payne, S., Richardson, D.J., Clarke, T.A. and Butt, J.N., (2018). Membrane-spanning electron transfer proteins from electrogenic bacteria: production and investigation. Methods Enzymol. 613, 257-275.

18. Edwards, M.J., White, G.F., Lockwood, C.W., Lawes, M.C., Martel, A., Harris, G., Scott, D.J., Richardson, D.J., Butt, J.N. and Clarke, T.A., (2018). Structural modeling of an outer membrane electron conduit from a metal-reducing bacterium suggests electron transfer via periplasmic redox partners. J. Biol. Chem. 293, 8103-8112.

19. van Wonderen, J.H., Adamczyk, K., Wu, X., Jiang, X.Y., Piper, S.E.H., Hall, C.R., Edwards, M.J., Clarke, T.A., Zhang, H., Jeuken, L.J.C., Sazanovich, I.V., Towrie, M., Blumberger, J., Meech, S.R. and Butt, J.N., (submitted). Nanosecond heme-to-heme electron transfer rates in a multiheme cytochrome nanowire reported by a spectrally unique His/Met ligated heme.

20. van Wonderen, J.H., Li, D.B., Piper, S.E.H., Lau, C.Y., Jenner, L.P., Hall, C.R., Clarke, T.A., Watmough, N.J. and Butt, J.N., (2018). Photosensitised multiheme cytochromes as light-driven molecular wires and resistors. ChemBioChem 19, 2206-2215.

21. Barr, I. and Guo, F., (2015). Pyridine hemochromagen assay for determining the concentration of heme in purified protein solutions. Bio Protoc. 5, e1594.

22. Demeler, B., UltraScan - A comprehensive data analysis software package for analytical ultracentrifugation experiments. In *Analytical Ultracentrifugation: Techniques and Methods*, Scott, D. J., Harding, S. E., and Rowe, A. J., Ed. Royal Society of Chemistry: Cambridge, UK, 2005.

23. Kline, S.R., (2006). Reduction and analysis of SANS and USANS data using IGOR Pro. J. Appl. Crystallogr. 39, 895-900.

24. Manalastas-Cantos, K., Konarev, P.V., Hajizadeh, N.R., Kikhney, A.G., Petoukhov, M.V., Molodenskiy, D.S., Panjkovich, A., Mertens, H.D.T., Gruzinov, A., Borges, C., Jeffries, C.M., Svergun, D.I. and Franke, D., (2021). ATSAS 3.0: expanded functionality and new tools for small-angle scattering data analysis. J. Appl. Crystallogr. 54, 343-355.

25. Svergun, D.I., (1992). Determination of the regularization parameter in indirect-transform methods using perceptual criteria. J. Appl. Crystallogr. 25, 495-503.

26. Franke, D. and Svergun, D.I., (2009). DAMMIF, a program for rapid ab-initio shape determination in small-angle scattering. J. Appl. Crystallogr. 42, 342-346.

27. Volkov, V.V. and Svergun, D.I., (2003). Uniqueness of *ab initio* shape determination in small-angle scattering. J. Appl. Crystallogr. 36, 860-864.

28. Svergun, D.I., (1999). Restoring low resolution structure of biological macromolecules from solution scattering using simulated annealing. Biophys. J. 76, 2879-2886.

29. Kozin, M.B. and Svergun, D.I., (2001). Automated matching of high- and low-resolution structural models. J. Appl. Crystallogr. 34, 33-41.

30. Pitre, S.P., McTiernan, C.D., Vine, W., DiPucchio, R., Grenier, M. and Scaiano, J.C., (2015). Visible-light actinometry and intermittent illumination as convenient tools to study $Ru(bpy)_3Cl_2$ mediated photoredox transformations. Sci. Rep. 5, 16397.

31. Hatchard, C.G. and Parker, C.A., (1956). A new sensitive chemical actinometer .2. Potassium ferrioxalate as a standard chemical actinometer. Proc. R. Soc. Lond. A Math. Phys. Sci. 235, 518-536.

32. Stikane, A., Hwang, E.T., Ainsworth, E.V., Piper, S.E.H., Critchley, K., Butt, J.N., Reisner, E. and Jeuken, L.J.C., (2019). Towards compartmentalized photocatalysis: multihaem proteins as transmembrane molecular electron conduits. Faraday Discuss. 215, 26-38.

33. Thomas, P.E., Ryan, D. and Levin, W., (1976). Improved staining procedure for detection of peroxidase-activity of cytochrome P-450 on sodium dodecyl-sulfate polyacrylamide gels. Anal. Biochem. 75, 168-176.

34. Martindale, B.C.M., Hutton, G.A.M., Caputo, C.A., Prantl, S., Godin, R., Durrant, J.R. and Reisner, E., (2017). Enhancing light absorption and charge transfer efficiency in carbon dots through graphitization and core nitrogen doping. Angew. Chem. 56, 6459-6463.

35. Rowe, S.F., Le Gall, G., Ainsworth, E.V., Davies, J.A., Lockwood, C.W.J., Shi, L., Elliston, A., Roberts, I.N., Waldron, K.W., Richardson, D.J., Clarke, T.A., Jeuken, L.J.C., Reisner, E. and Butt, J.N., (2017). Light-driven H_2 wvolution and C=C or C=O bond hydrogenation by *Shewanella oneidensis*: A versatile strategy for photocatalysis by nonphotosynthetic microorganisms. ACS Catal. 7, 7558-7566.

36. Geren, L., Hahm, S., Durham, B. and Millett, F., (1991). Photoinduced electron-transfer between cytochrome *c* peroxidase and yeast cytochrome *c* labeled at Cys-102 with (4-bromomethyl-4'-methylbipyridine)[bis(bipyridine)]Ruthenium^{2+}. Biochemistry 30, 9450-9457.

37. Millett, F. and Durham, B., (2002). Design of photoactive ruthenium complexes to study interprotein electron transfer. Biochemistry 41, 11315-11324.

38. van Wonderen, J.H., Hall, C.R., Jiang, X.Y., Adamczyk, K., Carof, A., Heisler, I., Piper, S.E.H., Clarke, T.A., Watmough, N.J., Sazanovich, I.V., Towrie, M., Meech, S.R., Blumberger, J. and Butt, J.N., (2019). Ultrafast light-driven electron transfer in a Ru(II)tris(bipyridine)-labeled multiheme cytochrome. J. Am. Chem. Soc. 141, 15190-15200.

39. Kokhan, O., Ponomarenko, N.S., Pokkuluri, P.R., Schiffer, M., Mulfort, K.L. and Tiede, D.M., (2015). Bidirectional photoinduced electron transfer in Ruthenium(II)-tris-bipyridyl-modified PpcA, a multi-heme *c*-type cytochrome from *Geobacter sulfurreducens*. J. Phys. Chem. B 119, 7612-7624.

40. Lebowitz, J., Lewis, M.S. and Schuck, P., (2002). Modern analytical ultracentrifugation in protein science: A tutorial review. Protein Sci. 11, 2067-2079.

41. Paradies, H.H., (1980). Shape and size of a non-ionic surfactant micelle. Triton X-100 in aqueous solution. J. Phys. Chem. 84, 599-607.

42. Edwards, M.J., White, G.F., Norman, M., Tome-Fernandez, A., Ainsworth, E., Shi, L., Fredrickson, J.K., Zachara, J.M., Butt, J.N., Richardson, D.J. and Clarke, T.A., (2015). Redox linked flavin sites in extracellular decaheme proteins involved in microbe-mineral electron transfer. Sci. Rep. 5, 11677

43. Jiang, X.Y., Burger, B., Gajdos, F., Bortolotti, C., Futera, Z., Breuer, M. and Blumberger, J., (2019). Kinetics of trifurcated electron flow in the decaheme bacterial proteins MtrC and MtrF. Proc. Natl. Acad. Sci. U.S.A. 116, 3425-3430.

44. Jiang, X.Y., van Wonderen, J.H., Butt, J.N., Edwards, M.J., Clarke, T.A. and Blumberger, J., (2020). Which multi-heme protein complex transfers electrons more efficiently? Comparing MtrCAB from *Shewanella* with OmcS from *Geobacter*. J. Phys. Chem. Lett. 11, 9421-9425.

45. Bose, A., Gardel, E.J., Vidoudez, C., Parra, E.A. and Girguis, P.R., (2014). Electron uptake by iron-oxidizing phototrophic bacteria. Nat. Commun. 5, 3391.

46. Chiranjeevi, P. and Patil, S.A., (2020). Strategies for improving the electroactivity and specific metabolic functionality of microorganisms for various microbial electrochemical technologies. Biotechnol. Adv. 39, 107468.

47. Hartshorne, R.S., Reardon, C.L., Ross, D., Nuester, J., Clarke, T.A., Gates, A.J., Mills, P.C., Fredrickson, J.K., Zachara, J.M., Shi, L., Beliaev, A.S., Marshall, M.J., Tien, M., Brantley, S., Butt, J.N. and Richardson, D.J., (2009). Characterization of an electron conduit between bacteria and the extracellular environment. Proc. Natl. Acad. Sci. U.S.A. 106, 22169-22174.

48. Castelle, C., Guiral, M., Malarte, G., Ledgham, F., Leroy, G., Brugna, M. and Giudici-Orticoni, M.T., (2008). A new iron-oxidizing/O_2-reducing supercomplex spanning both inner and outer membranes, isolated from the extreme acidophile *Acidithiobacillus ferrooxidans*. J. Biol. Chem. 283, 25803-25811.

49. Yarzabal, A., Brasseur, G., Ratouchniak, J., Lund, K., Lemesle-Meunier, D., DeMoss, J.A. and Bonnefoy, V., (2002). The high-molecular-weight cytochrome *c* Cyc2 of *Acidithiobacillus ferrooxidans* is an outer membrane protein. J. Bacteriol. 184, 313-317.

50. Gupta, D., Sutherland, M.C., Rengasamy, K., Meacham, J.M., Kranz, R.G. and Bose, A., (2019). Photoferrotrophs produce a PioAB electron conduit for extracellular electron uptake. mBio 10, e02668-19.

51. Li, D.B., Edwards, M.J., Blake, A.W., Newton-Payne, S.E., Piper, S.E.H., Jenner, L.P., Sokol, K.P., Reisner, E., Van Wonderen, J.H., Clarke, T.A. and Butt, J.N., (2020). His/Met heme ligation in the PioA outer membrane cytochrome enabling light-driven extracellular electron transfer by *Rhodopseudomonas palustris* TIE-1. Nanotechnology 31, 354002.

52. Liu, Y.M., Wang, Z.M., Liu, J., Levar, C., Edwards, M.J., Babauta, J.T., Kennedy, D.W., Shi, Z., Beyenal, H., Bond, D.R., Clarke, T.A., Butt, J.N., Richardson, D.J., Rosso, K.M., Zachara, J.M., Fredrickson, J.K. and Shi, L., (2014). A trans-outer membrane porin-cytochrome protein complex for extracellular electron transfer by *Geobacter sulfurreducens* PCA. Environ. Microbiol. Rep. 6, 776-785.

53. Ross, D.E., Flynn, J.M., Baron, D.B., Gralnick, J.A. and Bond, D.R., (2011). Towards electrosynthesis in *Shewanella*: Energetics of reversing the Mtr pathway for reductive metabolism. PLOS ONE 6, e16649.

694 54. Jin, M., Jiang, Y.M., Sun, L.L., Yin, J.H., Fu, H.H., Wu, G.F. and Gao, H.C., (2013). Unique
695 organizational and functional features of the cytochrome c maturation system in *Shewanella*
696 *oneidensis*. PLOS ONE 8, e75610.

697 55. Schicklberger, M., Bucking, C., Schuetz, B., Heide, H. and Gescher, J., (2011). Involvement
698 of the *Shewanella oneidensis* decaheme cytochrome MtrA in the periplasmic stability of the beta-
699 barrel protein MtrB. Appl. Environ. Microb. 77, 1520-1523.

700 56. Shi, L., Deng, S., Marshall, M.J., Wang, Z.M., Kennedy, D.W., Dohnalkova, A.C., Mottaz,
701 H.M., Hill, E.A., Gorby, Y.A., Beliaev, A.S., Richardson, D.J., Zachara, J.M. and Fredrickson, J.K.,
702 (2008). Direct involvement of type II secretion system in extracellular translocation of *Shewanella*
703 *oneidensis* outer membrane cytochromes MtrC and OmcA. J. Bacteriol. 190, 5512-5516.

704 57. Myers, J.M. and Myers, C.R., (2001). Role for outer membrane cytochromes OmcA and
705 OmcB of *Shewanella putrefaciens* MR-1 in reduction of manganese dioxide. Appl. Environ. Microb.
706 67, 260-269.

707 58. Fan, G., Dundas, C.M., Graham, A.J., Lynd, N.A. and Keitz, B.K., (2018). *Shewanella*
708 *oneidensis* as a living electrode for controlled radical polymerization. Proc. Natl. Acad. Sci. U.S.A.
709 115, 4559-4564.

710 59. Flynn, J.M., Ross, D.E., Hunt, K.A., Bond, D.R. and Gralnick, J.A., (2010). Enabling
711 unbalanced fermentations by using engineered electrode-interfaced bacteria. mBio 1, e00190-10.

712 60. Schuergers, N., Werlang, C., Ajo-Franklin, C.M. and Boghossian, A.A., (2017). A synthetic
713 biology approach to engineering living photovoltaics. Energy Environ. Sci. 10, 1102-1115.

714 61. Su, L. and Ajo-Franklin, C.M., (2019). Reaching full potential: bioelectrochemical systems
715 for storing renewable energy in chemical bonds. Curr. Opin. Biotech. 57, 66-72.

716

717 10 Supplementary Material

718 Method for estimation of liposome concentration, SDS-PAGE gels, spectral distribution of the light
719 sources, characterization of carbon dots, absorbance and photoluminescence spectra, SANS
720 scattering intensity profiles, statistical parameters associated with DAMMIN models and alignment
721 to homology model of MTR complex from *S. oneidensis*.

722

723

724 11 Data Availability Statement

725 The SANS data were deposited with SASBDB (http://www.sasbdb.org/) accession code *(to be added*
726 *once entry confirmed)*. Additional datasets can be found at the repository of the University of East
727 Anglia Research Data Base: https://people.uea.ac.uk/j_butt/datasets.

728

729

730 Figure Legends

Fig. 1. The MTR complex of *Shewanella*.

(A) Schematic of the electron transfer pathway in *S. oneidensis* MR-1 from menaquinol (MQH_2) to external terminal respiratory electron acceptors. (B) Model for the MTR complex of *S. oneidensis* MR-1 based on the crystal structure[15] of *S. baltica* MTR complex. MtrAB (gray) showing the hemes (red). MtrC (tan) illustrating the location of the hemes (purple) and Tyr657 (blue). Hemes numbered according to their order of attachment to the primary sequence. Image rendered with Chimera. (C) Schematic of the *in vitro* association of MtrC and MtrAB (above) and trans-membrane electron transfer (below) through the resultant MtrC:MtrAB complex in proteoliposomes carrying the azo-dye cargo (black hexagons).

Fig. 2. Biophysical Characterization of Ru-MtrC:MtrAB.

(A) Sedimentation equilibrium analytical ultracentrifugation traces for 0.4 μM MtrAB (black), 0.4 μM Ru-MtrC (red) and a mixture of 0.25 μM Ru-MtrC equilibrated with 0.25 μM MtrAB (blue). Samples were centrifuged at 8k rpm for 20 h at 20℃ in 50 mM sodium phosphate, 50 mM NaCl, 0.1% (v/v) Triton X-100, pH 7.5 to reach equilibrium. Lower panel: data (circles) and fits (lines) to the behavior for a single non-interacting species, see text for details. Upper panel: residuals. (B) Gel filtration chromatograms for samples of 40 μM MtrAB (black), 40 μM Ru-MtrC (red) and a mixture of 32 μM Ru-MtrC equilibrated with 48 μM MtrAB (blue). A Superose 6 Increase 10/300 column was equilibrated in 50 mM sodium phosphate, 50 mM NaCl, 5 mM LDAO, pH 7.5. Elution was at 0.25 mL min^{-1}. (C) SDS-PAGE analysis of the MTR complex (①) and Ru-MtrC:MtrAB (②) (V_e <16.5 mL from gel filtration shown in Panel B). Proteins visualized by Coomassie and Heme stain as indicated.

Fig. 3. Analysis of SANS Data for Ru-MtrC:MtrAB

(A) Scattering data (truncated to Q = 0.161) shown as circles with the fit to the P(r) curve generated by GNOM shown as a line. (B) Guinier region of scattering curve, lower panel shows data as circles and a linear fit as a line. Upper panel shows residuals from fitting. (C) Kratky plot. (D) P(r) distance distribution curve. (E) Molecular envelope of Ru-MtrC:MtrAB (blue mesh) generated by DAMMIN aligned with the homology model of the MTR complex from *S. oneidensis* (gray with red hemes). (F) Molecular envelope of Ru-MtrC:MtrAB (blue mesh) aligned with that of the MTR complex (orange mesh). Source data for latter as reported in Ref.[16] see text for details.

Fig. 4. Photoreduction of Ru-MtrC and Ru-MtrC:MtrAB Suspensions.

Spectra of oxidized protein (thick colored line), over 90 min irradiation (thin colored lines) and after addition of dithionite (black line) for (A) Ru-MtrC and (B) Ru-MtrC:MtrAB. Samples of Ru-MtrC (0.12 μM) and Ru-MtrC:MtrAB (0.14 μM) in anaerobic 50 mM Tris, 10 mM KCl, 100 mM EDTA, 0.2% (v/v) Triton X-100, pH 8.5. Irradiation at 450 nm, intensity 110 W m^{-2}. (C) Time course of photoreduction for Ru-MtrC (red) and Ru-MtrC:MtrAB (blue). Number of reduced hemes defined by $\Delta A_{420\ nm}$, see text for details.

Fig. 5. Characterization of (Proteo-)Liposomes.

Size analysis by dynamic light scattering of RR120-containing liposomes with Ru-MtrC:MtrAB (blue), the MTR complex (red), or no proteins (gray). Proteoliposome concentrations estimated at 6 nM in 50 mM Tris:HCl, 10 mM KCl, pH 8.5. Inset shows Coomassie-stained SDS-PAGE gel loaded with the MTR complex (①); RR120-containing proteoliposomes with the MTR complex (②) or Ru-MtrC:MtrAB (③); RR120-containing liposomes (④). Pre-stained protein ladder as in Fig. 2C.

Fig. 6. Dithionite driven electron transfer across Ru-MtrC:MtrAB containing liposome bilayers.

(A-C) Spectra of 6 nM (proteo-)liposomes containing RR120 with indicated proteins before (thick line) and over 30 min following addition of 0.1 mM dithionite (thin lines); arrows indicate bleaching of RR120. Samples in 50 mM Tris:HCl, 10 mM KCl, pH 8.5. Raleigh scattering due to liposomes has been subtracted, see text for details. (D) Time course for bleaching of encapsulated RR120 from panels A-C with data points connected for clarity. Data are the average of $n = 3$ data sets and error bars show standard deviation.

Fig. 7. Light-driven electron transfer across Ru-MtrC:MtrAB containing liposome bilayers with graphitic N-doped Carbon Dots.

(A-C) Spectra of 6 nM (proteo-)liposomes containing RR120 with indicated proteins before (thick line) and over 15 min irradiation (thin lines) with visible light (2.5 kW m^{-2}); arrows indicate reduction of hemes and bleaching of RR120. Samples in 50 mM Tris:HCl, 10 mM KCl, 25 mM EDTA, 10 µg mL^{-1} graphitic N-doped Carbon Dots, pH 8.5. Scattering contributions from Carbon Dots and liposomes have been subtracted as described in Methods. (D) Time course showing bleaching of encapsulated RR120 in (proteo-)liposomes from panels A-C with data points connected for clarity. Data are the average of $n = 3$ data sets and error bars show standard deviation.

Fig. 8. **Harnessing the MTR complex to couple internal (biological) and external (synthetic) catalysts in a closed redox cycle.**

(A) *S. oneidensis* as a living electrode driving an exogenous copper-based catalyst to produce radicals, these initiate olefin polymerisation[58]. (B) *S. oneidensis* performing electrode-assisted glycerol oxidation[59]. (C) A strategy to engineer bacteria for semi-artificial photosynthesis motivated by this work; soluble MtrC is functionalized with a photo-electrocatalyst and then assembles spontaneously with bacteria presenting MtrAB in their outer membrane; allowing intracellular substrate oxidation to be coupled to extracellular photo-electrocatalysis.

805 Figure 1.

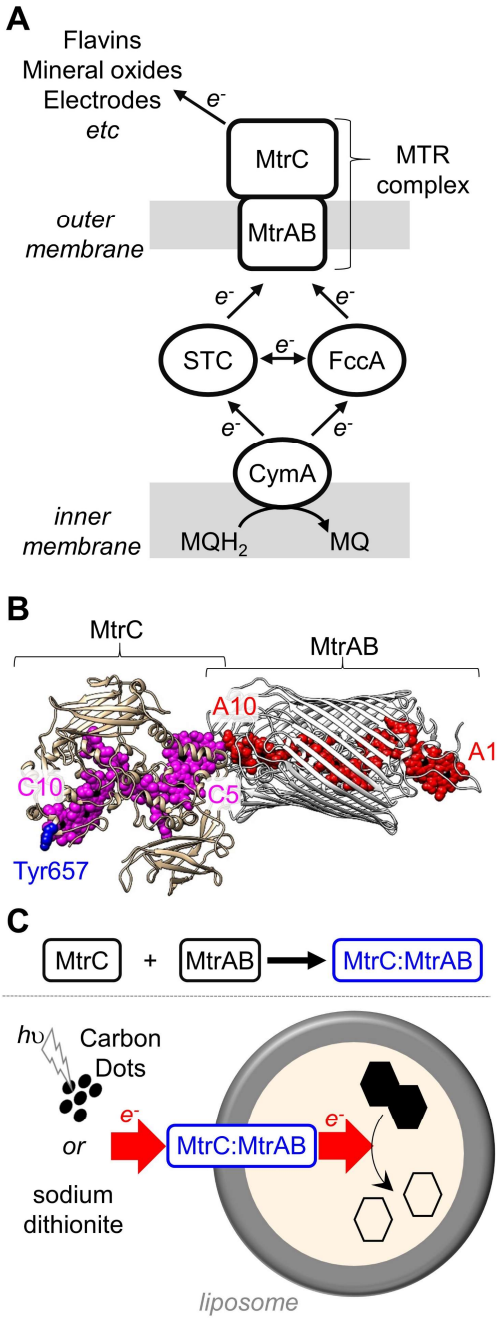

806

807 Figure 2

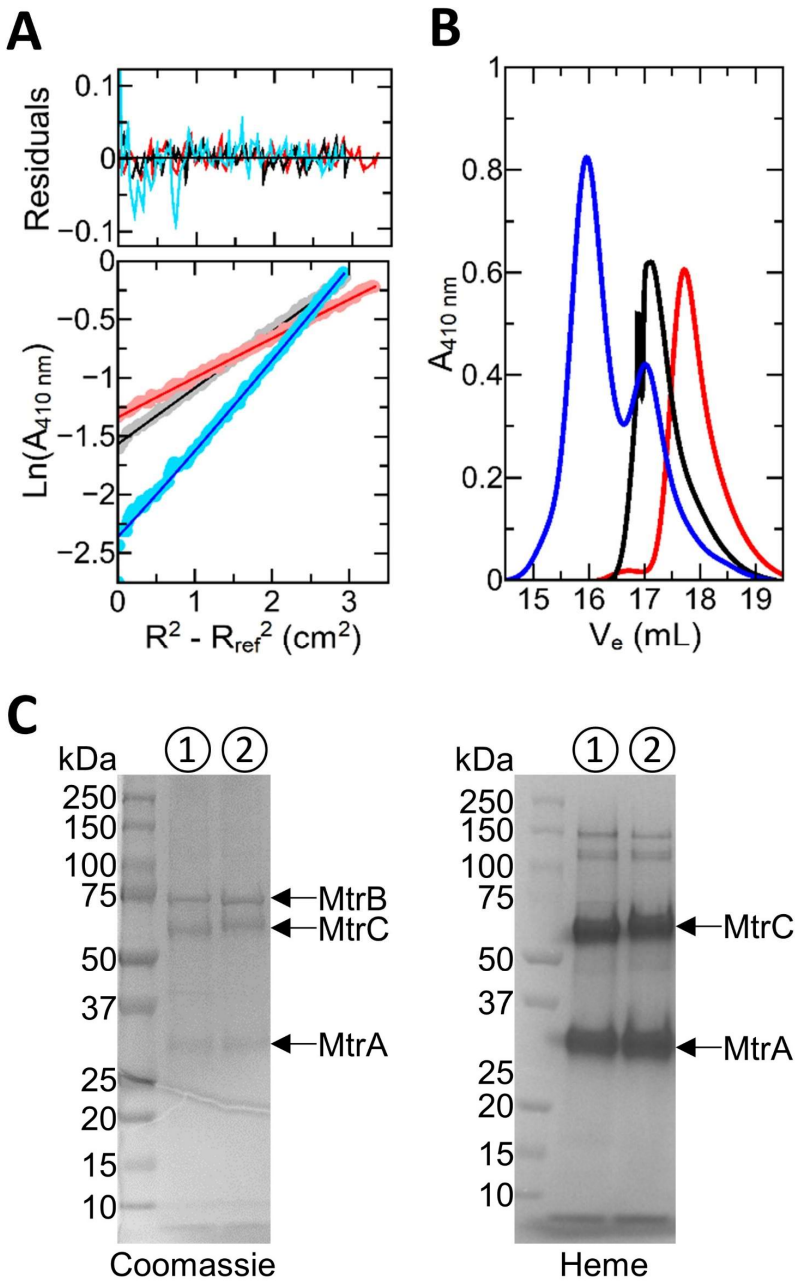

808

809 Figure 3

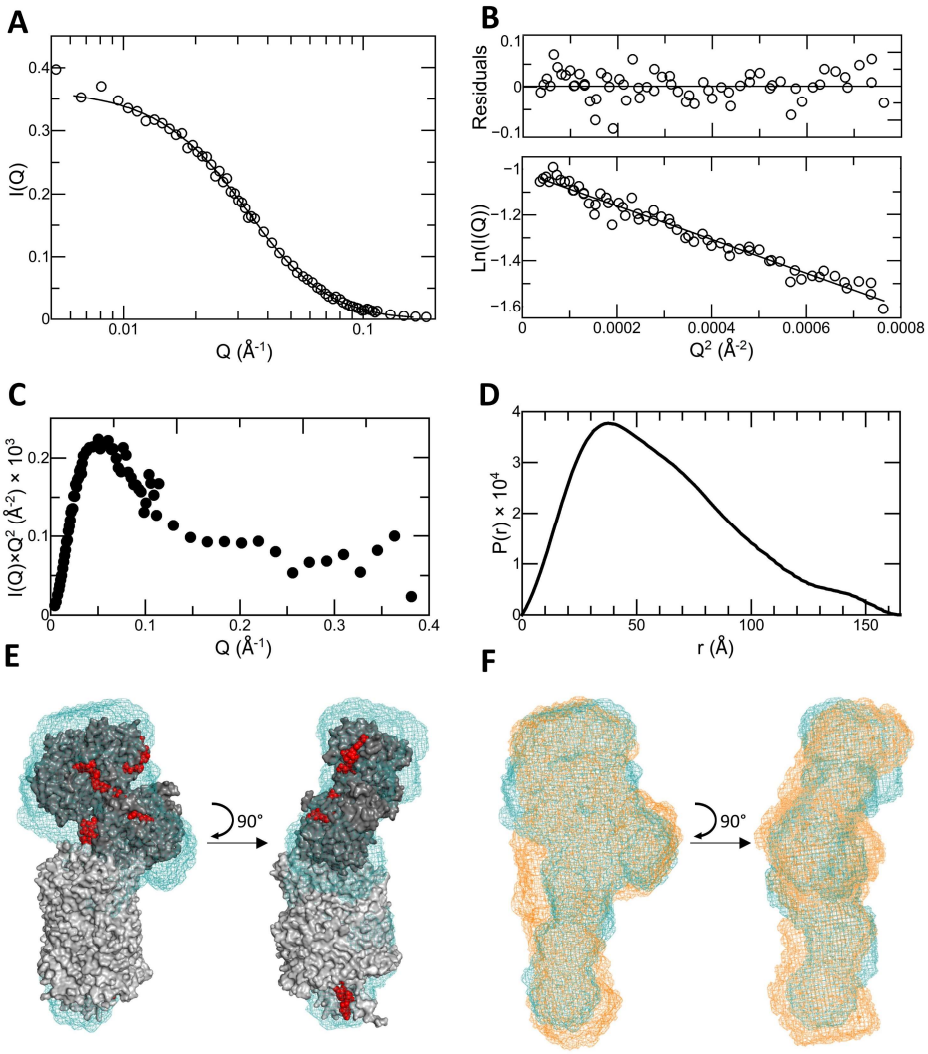

810

811 Figure 4

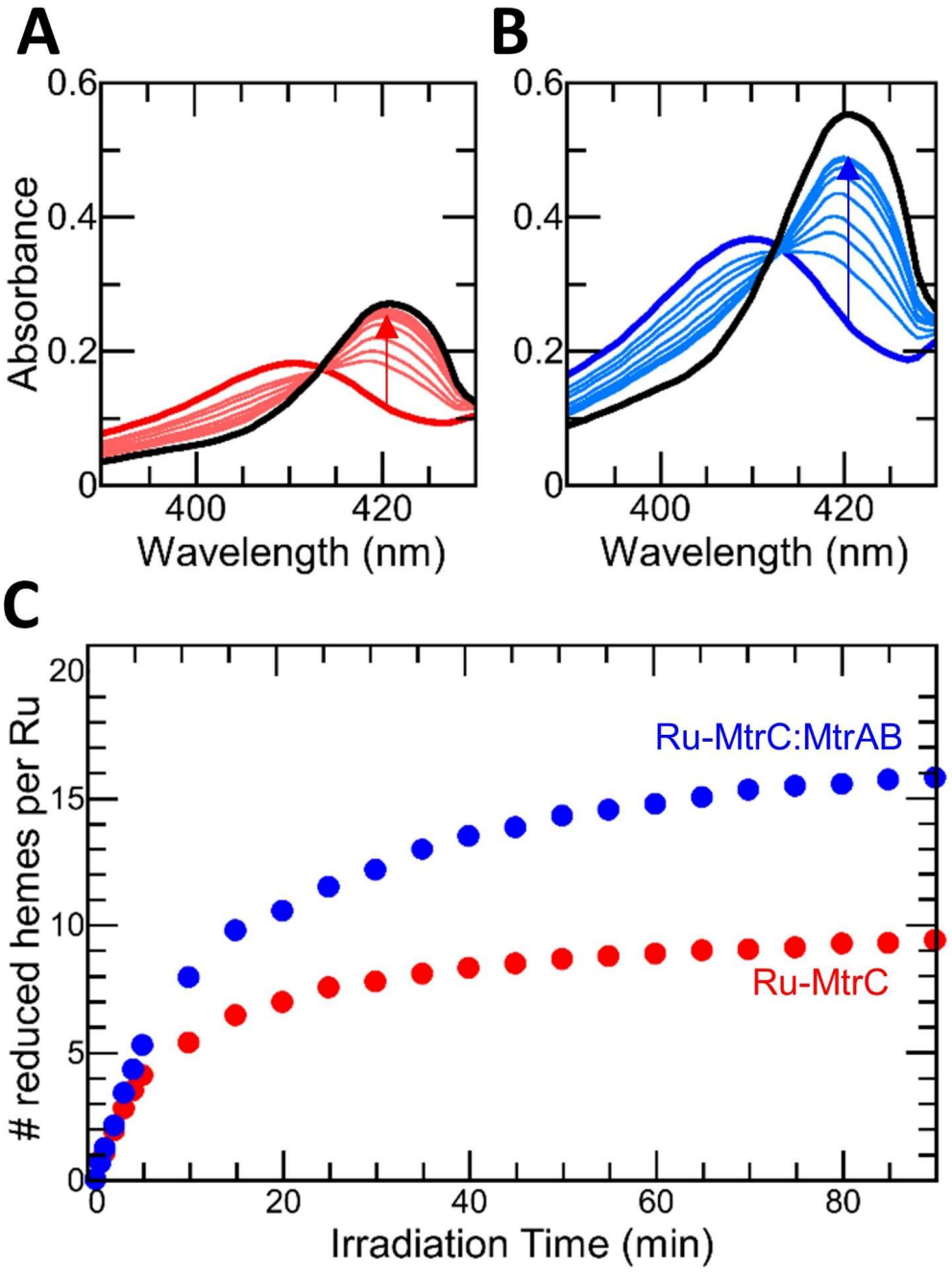

812

813 Figure 5

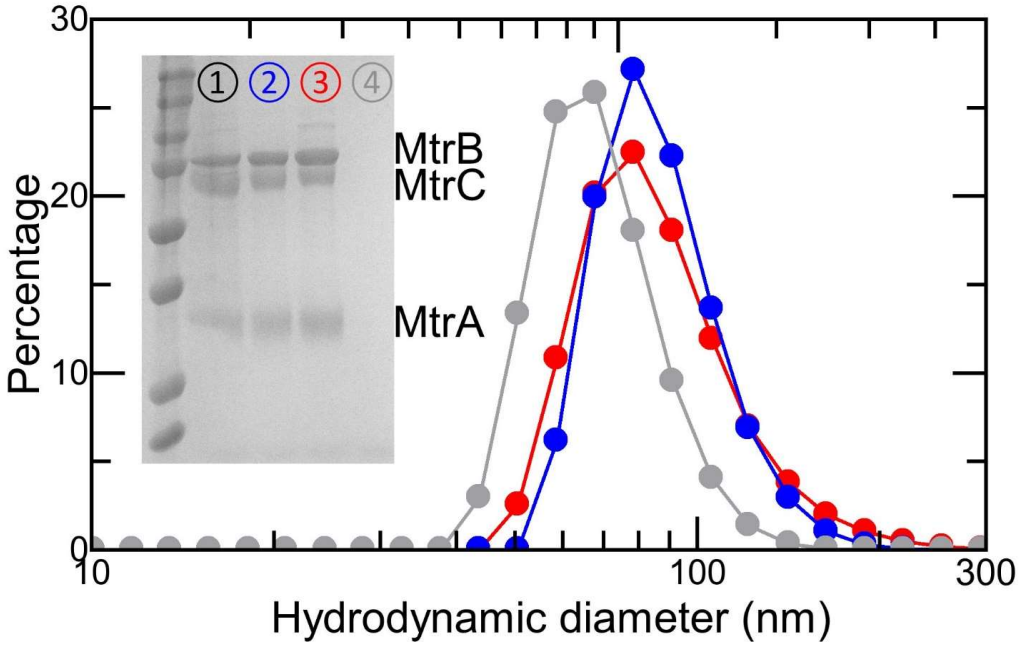

814

815

816 Figure 6

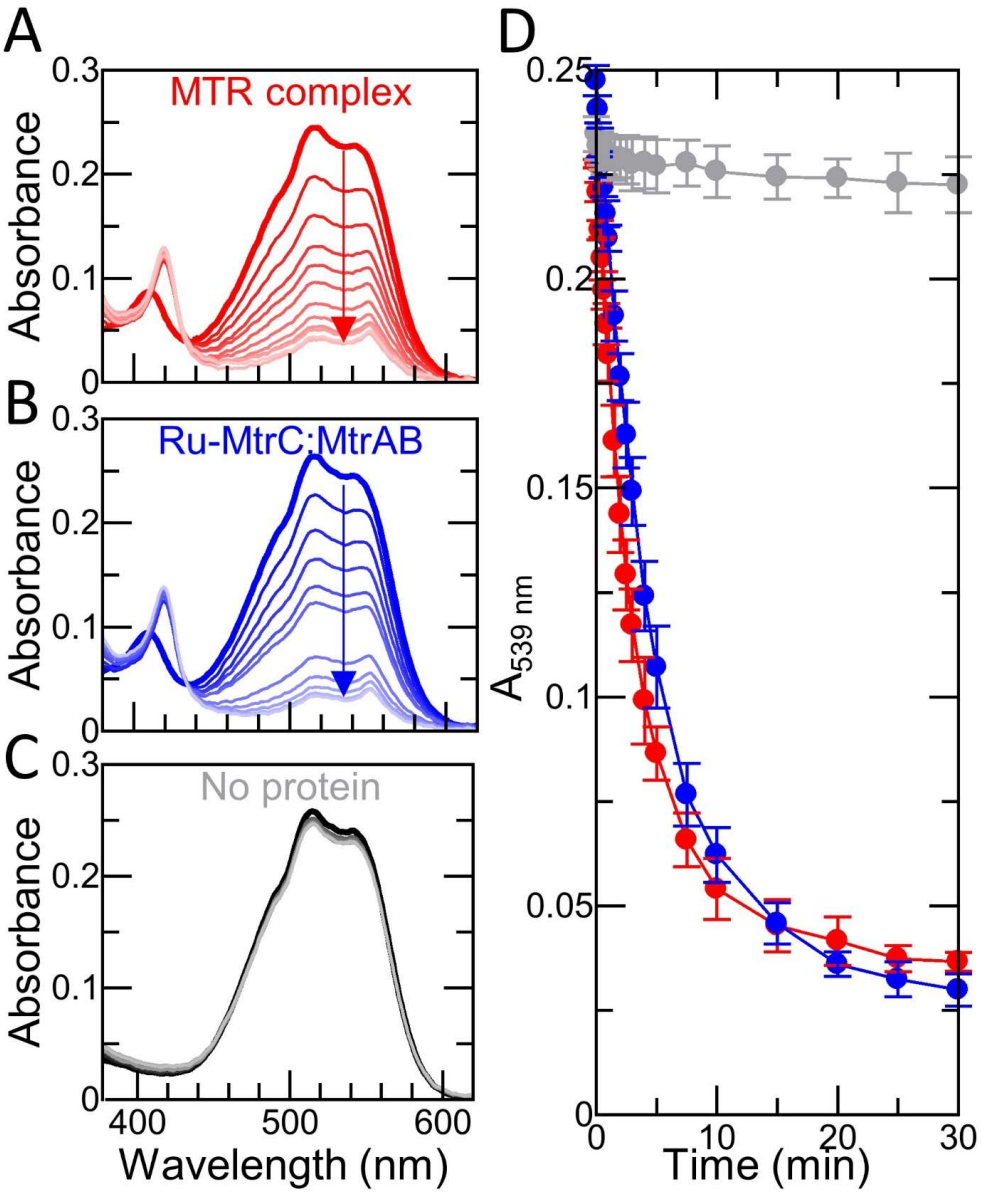

817

818 Figure 7

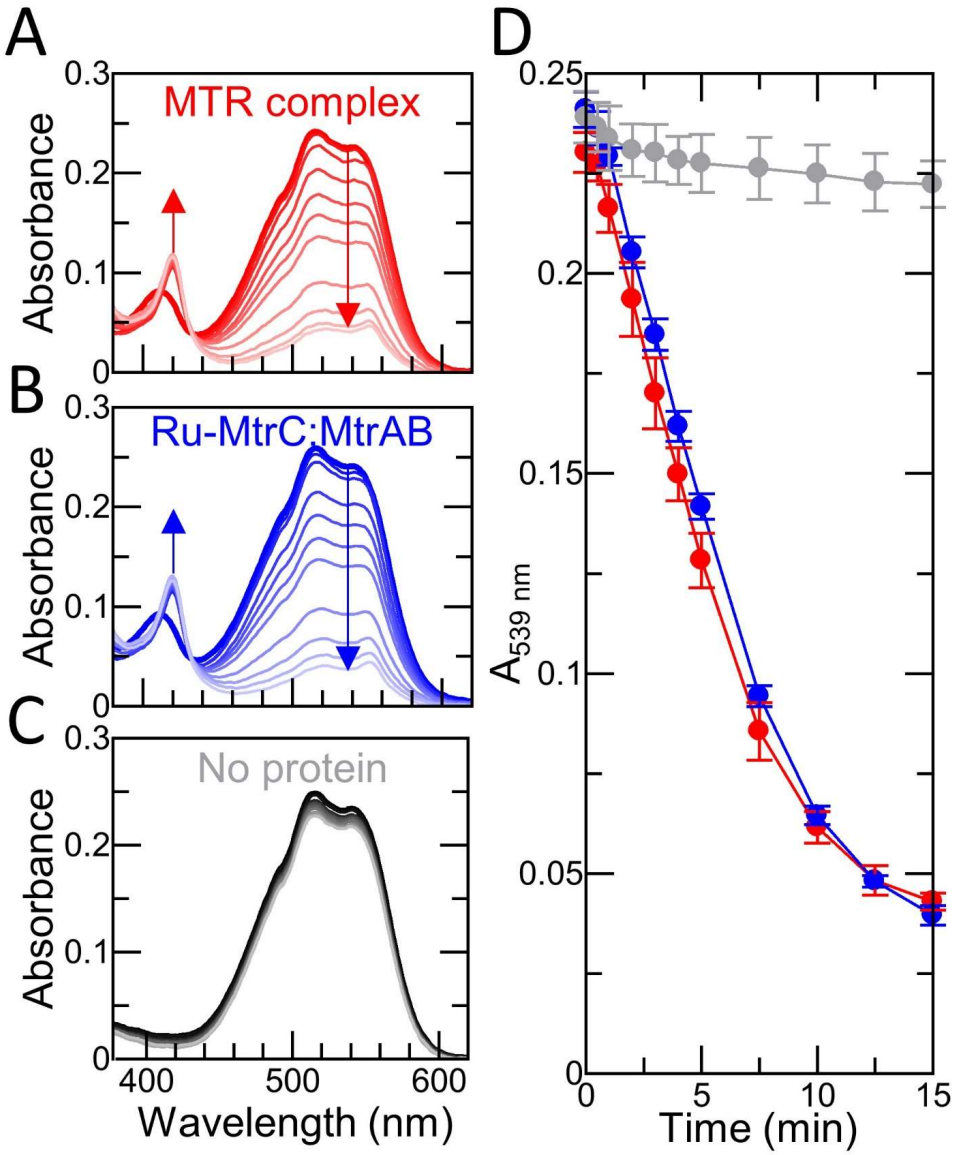

819

820 Figure 8

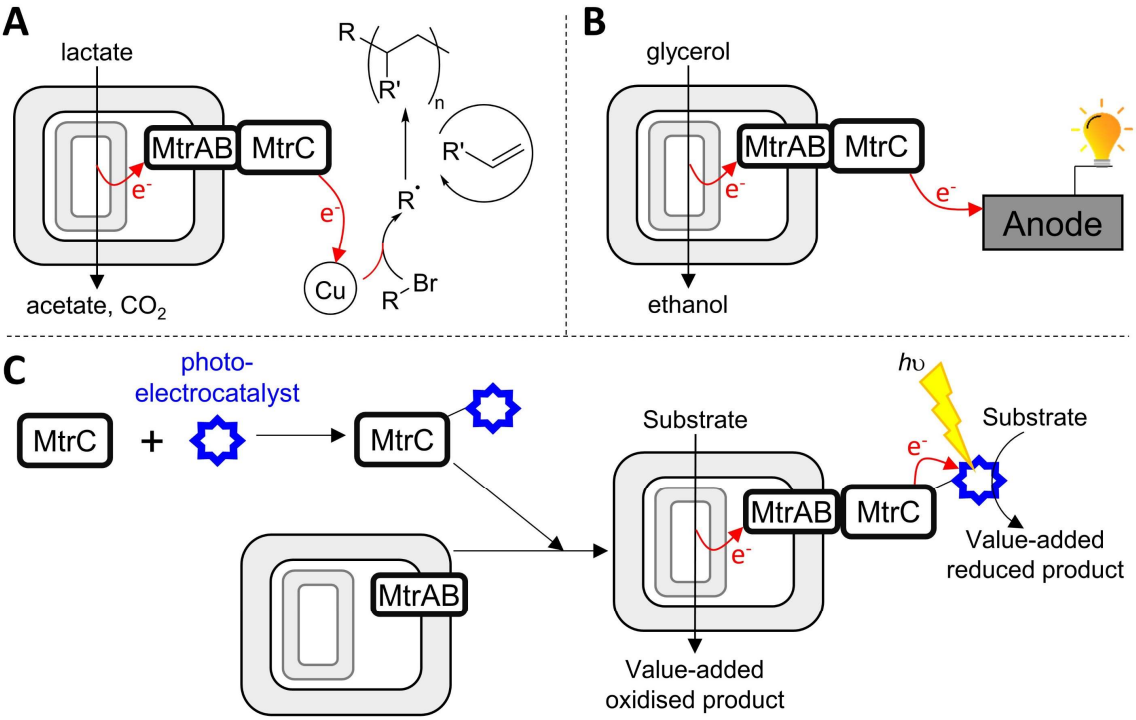

821